Numerical and Laboratory Study of a Horizontally Evolving Convective Boundary Layer. Part I: Transition Regimes and Development of the Mixed Layer

E. FEDOROVICH

Institute for Hydromechanics, University of Karlsruhe, Karlsruhe, Germany

F. T. M. NIEUWSTADT

J. M. Burgers Centre for Fluid Mechanics, Delft University of Technology, Delft, Netherlands

R. KAISER

Zeuna Stärker GmbH and Company, KG, Augsburg, Germany

(Manuscript received 7 July 1999, in final form 26 April 2000)

ABSTRACT

Results are presented from a large eddy simulation (LES) and wind tunnel study of the turbulence regime in a horizontally evolving sheared atmospheric convective boundary layer (CBL) capped by a temperature inversion. The wind tunnel part of the study has been conducted in the thermally stratified tunnel of the University of Karlsruhe. For the numerical part a modified LES procedure that was originally designed for simulation of the horizontally homogeneous atmospheric CBL has been employed.

The study focuses on the transition between the neutrally buoyant boundary layer in the initial portion of the wind tunnel flow and a quasi-homogeneous convectively mixed layer developing downwind. The character of the transition between the two boundary layers and the associated changes in the turbulence structure are found to be strongly dependent on the magnitude and distribution of disturbances in the flow at the entrance of the wind tunnel test section. For all simulated inflow conditions, the transition is preceded by accumulation of potential energy in the premixed CBL. The eventual energy release in the transition zone leads to turbulence enhancement that has a form of turbulence outbreak for particular flow configurations.

The numerically simulated CBL case with temperature fluctuations introduced in the lower portion of the incoming flow appears to be the closest to the basic CBL flow case studied in the wind tunnel. Second-order turbulence statistics derived from the LES are shown to be in good agreement with the wind tunnel measurements. Main features of transition, including the turbulence enhancement within the transition zone, are successfully reproduced by the LES.

1. Introduction

A buoyancy driven convective boundary layer (CBL) heated from below and capped by a density interface (the so-called inversion layer) is commonly observed in the atmosphere during daytime conditions. In the absence of mean wind (the case of shear-free convection), turbulence in the CBL is solely maintained by buoyancy production at the heated underlying surface. The buoyant forcing favors vertical motions and leads to the characteristic cellular convection pattern composed of warm updrafts (thermals) and associated cool downdrafts. In the presence of mean wind, the CBL turbulence regime is modified by flow shears at the surface and across the inversion layer at the CBL top.

Most numerical and laboratory studies carried out so far have assumed statistical quasi homogeneity of the CBL over a horizontal plane and regarded the CBL evolution as a nonstationary (or nonsteady) process. Available measurement data on the convective turbulence structure in the atmosphere usually also refer to this CBL type. Another type of the atmospheric CBL is the horizontally evolving CBL, which grows in a neutrally or stably stratified air mass that is advected over a heated underlying surface. Properties of turbulence in this type of the CBL are much less known compared to the nonstationary, horizontally homogeneous CBL case.

A thermally stratified wind tunnel was constructed at the University of Karlsruhe (UniKa) by Rau and Plate (1995) to study the quasi-stationary, horizontally evolving CBL. A series of experiments has been carried out

Corresponding author address: Dr. Evgeni Fedorovich, School of Meteorology, University of Oklahoma, Energy Center, 100 East Boyd, Norman, OK 73019-1013.
E-mail: fedorovich@ou.edu

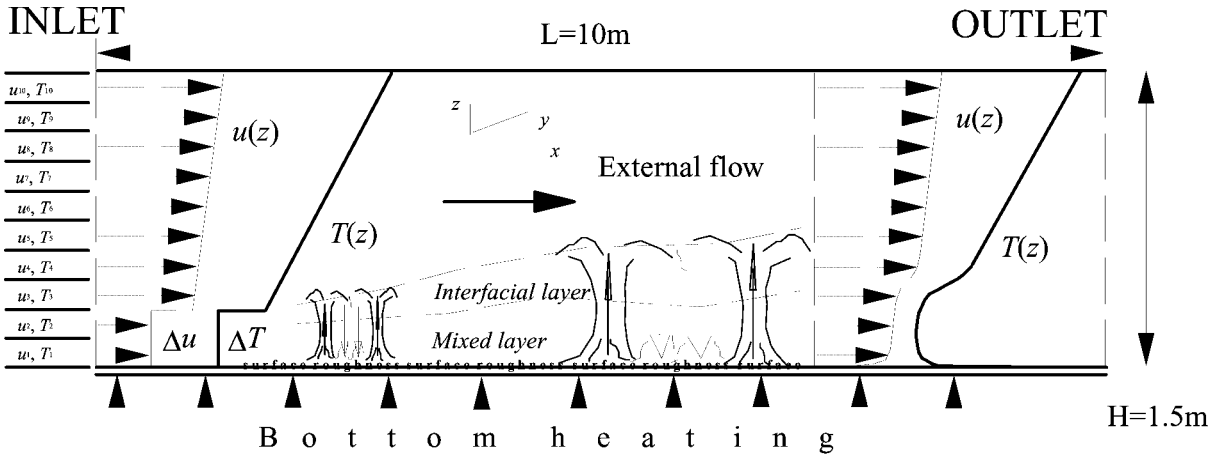

FIG. 1. Sketch of simulation domain (the wind tunnel test section) with the evolving CBL.

in this tunnel during the last several years aimed at a comprehensive investigation of the turbulence structure in the sheared CBL. Results of these experiments have been reported in Fedorovich et al. (1996), Kaiser and Fedorovich (1998), and Fedorovich and Kaiser (1998). The experiments have shown that wind shears can substantially modify the CBL turbulence dynamics. The buoyancy appeared to be the dominant mechanism of turbulence production at larger scales of motion, while the role of shear was increasing toward the range of smaller scales. Measurements in the tunnel also gave an indication that wind shear across the inversion layer can attenuate the entrainment process and thus affect the CBL growth.

In the course of the aforementioned experiments it became clear that laboratory measurements should be complemented with numerical simulations in order to better understand and quantitatively describe the evolution of turbulence regime in the horizontally inhomogeneous CBL. Such a combination of physical experiment and numerical simulation was the main guiding idea of the present study. A similar combined approach has been recently applied in the CBL studies of Ohya et al. (1998) and Ohya and Uchida (1999).

Large eddy simulation (LES), which is used as numerical technique in our study, has been extensively employed in the atmospheric research to reproduce various cases of the nonsteady, horizontally homogeneous CBL. Among the most well-known LES codes designed for this purpose are those of Deardorff (1972), Moeng (1984), Wyngaard and Brost (1984), Nieuwstadt and Brost (1986), Mason (1989), and Schmidt and Schumann (1989). These codes are based on the same prognostic equations but use different numerical algorithms and parameterizations of subgrid turbulence. The comparative study of the four representative atmospheric LES codes by Nieuwstadt et al. (1993) has demonstrated that results of their predictions are consistent with each other, at least for the CBL cases with dominant buoyant forcing.

For the present study, the LES code described by Nieuwstadt and Brost (1986) and Nieuwstadt (1990) has been modified in order to allow the simulation of a spatially evolving CBL. The modified LES procedure is described in section 2 of this paper, where also the basic features of the wind tunnel experiments are briefly reviewed. The LES results for the CBL cases with different inflow conditions are shown and discussed in section 3. Longitudinal evolution of mixing and entrainment in the developing CBL is analyzed in section 4 based both on the wind tunnel measurements and the LES data. Summarizing remarks and conclusions are presented in section 5.

2. Simulation techniques

a. Laboratory simulation

The UniKa wind tunnel is specially designed for simulating the inversion-capped CBL developing over a heated underlying surface (Rau and Plate 1995). The tunnel is of close-circuit type, with a 10 m $\times$ 1.5 m $\times$ 1.5 m test section. The return section of the tunnel is subdivided into 10 individually insulated layers. Each layer is driven by its own fan and heating system. This allows preshaping of the velocity and temperature profiles at the inlet of the test section as shown in Fig. 1. A feedback control system enforces quasi-stationary inlet conditions for the flow entering the test section. The test section floor, which is constructed of aluminum plates, can be also heated with a controlled energy input to produce a constant heat flux through the underlying surface.

The components of flow velocity in the tunnel are measured with a laser Doppler velocimetry (LDV), which provides a highly accurate observation of flow at a single measurement location. For temperature measurements, a resistance-wire technique is employed. During the simultaneous temperature and velocity measurements, the LDV measurement volume and the tem-

perature probe are placed at the same height with the temperature probe shifted 1 mm downstream in order to avoid disturbances of the velocity field.

In addition to the velocity and temperature measurements, a laser light sheet technique is applied to observe two-dimensional flow patterns on planes oriented along various directions with respect to the flow. Detailed information about the flow measurement and visualization technique employed in the tunnel is presented in Kaiser and Fedorovich (1998), and Fedorovich and Kaiser (1998), where also the accuracy of the flow measurements is discussed.

b. LES technique

In LES, one solves a system of equations for the filtered (resolved) flow fields given by

$$\frac{\partial \overline{u}_i}{\partial t} + \frac{\partial \overline{u}_j \overline{u}_i}{\partial x_j} = -\frac{\partial \pi}{\partial x_i} + \beta(\overline{T} - T_0)\delta_{i3} + \frac{\partial}{\partial x_j}\left[\nu\left(\frac{\partial \overline{u}_i}{\partial x_j} + \frac{\partial \overline{u}_j}{\partial x_i}\right) - \tau_{ij}\right], \quad (1)$$

$$\frac{\partial \overline{u}_i}{\partial x_i} = 0, \quad (2)$$

$$\frac{\partial \overline{T}}{\partial t} + \frac{\partial \overline{u}_i \overline{T}}{\partial x_i} = \frac{\partial}{\partial x_i}\left(\mu \frac{\partial \overline{T}}{\partial x_i} - Q_i\right), \quad (3)$$

where t stands for the time, $x_i = (x, y, z)$ are the right-hand Cartesian coordinates, $\overline{u}_i = (\overline{u}, \overline{v}, \overline{w})$ are the filtered (resolved) components of the velocity vector, $\overline{T}$ is the filtered temperature, T_0 is the reference temperature, ν is the kinematic viscosity, and μ is the molecular thermal diffusivity. The quantities $\tau_{ij} = \overline{u_i u_j} - \overline{u}_i \overline{u}_j$ and $Q_i = \overline{T u_i} - \overline{T}\,\overline{u}_i$ are the subgrid stress and subgrid heat flux, respectively, and $\beta = g/T_0$ is the buoyancy parameter, where g is the gravity acceleration. The overbar signifies the average over the grid-cell volume, which in our case is taken to be the filter procedure. The prime denotes the deviation from the average value. The normalized pressure π in Eq. (1) is defined as

$$\pi = \frac{\overline{p} - p_0}{\rho_0},$$

where $\overline{p}$ is the filtered pressure; p_0 and ρ_0 are the reference values of pressure and density, respectively. The Boussinesq approximation is used in Eq. (1) to account for the influence of the buoyancy forcing. The Coriolis force, which is usually not important in the atmospheric CBL and which is negligible in the wind tunnel CBL (Fedorovich et al. 1996), is omitted in Eq. (1).

The subgrid stress and heat flux have been parameterized in terms of an eddy viscosity and eddy diffusivity model. We have followed the subgrid closure model proposed by Deardorff (1980), where the eddy viscosity K_m and diffusivity K_h are expressed through the mixing length l and subgrid kinetic energy E:

$$K_m = 0.12 l E^{1/2}, \qquad K_h = (1 + 2l/\Delta)K_m, \quad (4)$$

where $\Delta = (\Delta x \Delta y \Delta z)^{1/3}$ is the effective grid spacing and the mixing length is evaluated depending on the local temperature gradient as

$$l = \begin{cases} \Delta & \text{if } \partial\overline{T}/\partial z \le 0, \\ \min\{\Delta, 0.5E^{1/2}/[\beta(\partial\overline{T}/\partial z)]^{1/2}\} & \text{if } \partial\overline{T}/\partial z > 0. \end{cases} \quad (5)$$

The subgrid kinetic energy E has been obtained from a supplementary balance equation. For further details regarding the subgrid closure we refer to Nieuwstadt and Brost (1986) and Nieuwstadt et al. (1993), who have shown the adequacy of the employed subgrid model for simulation of the convective flows with dominant buoyant forcing.

In order to simplify further mathematical notation, the filtered or resolved velocity components $\overline{u}_1$, $\overline{u}_2$, $\overline{u}_3$, and temperature $\overline{T}$ will be hereafter denoted as u, v, w, and T, respectively.

The main part of original numerical solver has been preserved in the modified version of the code. The modification primarily involved the reformulation of the boundary conditions and revision of the numerical algorithm for solving the Poisson pressure equation in order to accommodate the nonperiodic sidewalls. Adjustment of the velocity fields to enforce the conservation of mass in the simulated flow is realized by the pressure. A Poisson equation for π is constructed by combining the continuity and momentum balance equations as is done in Nieuwstadt (1990). This Poisson equation is solved numerically by the fast Fourier transform technique over the horizontal planes and by a tridiagonal matrix decomposition in the vertical. In the Fourier series expansions, only cosine functions are used to enable matching the Neumann boundary conditions at the sidewalls.

The LES equations (1)–(3) are discretized in the rectangular domain (the UniKa tunnel test section) on a staggered grid with uniform spacing. In this domain, a right-hand coordinate system is defined with the longitudinal axis x directed from the inlet to the outlet, y oriented perpendicular to the flow, and the vertical axis z directed upward from the floor to the ceiling; see Fig. 1. The grid consists of standard $200 \times 30 \times 30$ cubic cells with an effective grid spacing $\Delta = 5$ cm. The spatial discretization on the grid is of the second order in space. The time advancement is carried out by means of the leapfrog explicit time integration scheme with a weak time filter.

We assume that with the effective grid spacing specified above the dominant portion of energy-containing turbulent motions in the simulated CBL is explicitly resolved. This assumption is based on the estimates by Kaiser and Fedorovich (1998) of the integral length scale, the Taylor microscale, and the Kolmogorov mi-

croscale in the wind tunnel CBL. They are, respectively, 50, 1, and 0.1 cm. The Taylor microtimescale is about 0.1 s, the convective turnover timescale is about 2 s, and the flow deformation timescale is of the order of 50 s.

Several LES test runs have been carried out at a twice higher resolution, that is, with a $400 \times 60 \times 60$ grid ($\Delta = 2.5$ cm). These runs consume considerable processor time, about 120 h per run, and could therefore be performed only in a limited number of cases. The solutions obtained with the higher-resolution simulations for the mean flow parameters and turbulence statistics are found to be very close to the simulation results with the standard grid.

With respect to boundary conditions, we try to simulate as realistically as possible the actual conditions in the test section of the UniKa wind tunnel. At the sidewalls and at the ceiling of the test section, no-slip boundary conditions for the velocity and zero-gradient conditions for the temperature, subgrid energy, and pressure are enforced. The log-wall law is employed to calculate local near-wall turbulent shear stresses, through which the mechanical production of E at the wall is expressed. At the heated bottom surface, the Monin–Obukhov similarity relations are used point by point to couple local thermal and dynamic parameters of the flow. The roughness lengths of walls, floor, and ceiling of the domain are set as external parameters.

The values of u, v, w, and T at the test section inlet (the inflow boundary) are prescribed. These inlet values are decomposed in two parts. The first part (the stationary part) is a steady value corresponding to the settings of the tunnel control system for each particular flow configuration. The stationary parts of u and T are given as output of control system, and the stationary parts of v and w are set equal to zero. The second part represents a nonstationary fluctuating component of the inflow. These fluctuations are prescribed as normally distributed noncorrelated random values with a given variance, which is estimated from the measured temperature and velocity fluctuations at the first measurement location (window) in the tunnel (see section 3).

The outlet boundary condition should provide an undisturbed removal of momentum and heat from the physical domain. For this the radiation boundary condition, also called the convective (or advective) boundary condition, is used. The numerical formulation of this condition is schematically presented as

$$\frac{\varphi_n^{(i+1)} - \varphi_n^{(i-1)}}{2\Delta t} + u_n^{(i-1)} \cdot \frac{\varphi_n^{(i-1)} - \varphi_{n-1}^{(i-1)}}{\Delta x} = 0,$$

where φ is a given prognostic variable, the superscript in brackets denotes the time level, and n is the number of the last grid cell in the x direction. For the pressure field, the Neumann boundary condition is prescribed at both inlet and outlet.

3. Flow evolution with different conditions at the inlet

a. Simulated cases

A series of numerical simulations have been conducted to determine the effect of the modified boundary conditions and to investigate the response of the turbulence regime in the simulated CBL to the disturbances at the domain inlet.

The conducted numerical simulations are separated into two groups. The first group comprises LES test runs, which have been carried out to identify most appropriate simulation configurations for reproducing the basic wind tunnel flow case described in Fedorovich et al. (1996). The second group includes numerical simulations performed to study different forcing mechanisms affecting the mean flow and turbulence structure in the horizontally inhomogeneous CBL as found in the laboratory experiments. The results of the second group are presented in a separate paper (Fedorovich et al. 2001).

In the basic experimental configuration of the wind tunnel, the two lower layers of the tunnel, with a depth of 0.3 m in total, operate in the open-circuit regime. The incoming flow in these two layers possesses the temperature of the ambient air (about 300 K). The kinematic heat flux through the bottom of the test section is kept constant, at the level of approximately 1 K m s^{-1}. Between the second and the third layers a 30-K temperature jump is imposed. The temperature of each of the subsequent layers is controlled in the way to produce a temperature gradient of 33 K m^{-1} (5 K per layer) in the upper flow region. The flow velocity in all layers at the inlet is set equal to 1 m s^{-1}. The same set of inflow parameters has been prescribed for the stationary flow component at the inlet of the LES domain (see section 2).

The values of the external parameters in the LES experiments have been set as follows. For the roughness length for momentum at the bottom surface we take $z_{0b} = 0.0001$ m. The same value is used for the roughness length for momentum at the walls and at the ceiling. For the inlet value of the subgrid energy we take $E_{ui} = 0.01$ m^2 s^{-2} under the temperature inversion and $E_{ai} = 0.001$ m^2 s^{-2} above the temperature inversion.

The LES case with the settings specified above and with no imposed velocity and temperature disturbances at the inlet will be hereafter referred to as the stationary (ST) case. Other simulation configurations to be considered are distinguished by a nonstationary inflow component with given magnitude and spatial distribution of velocity and temperature fluctuations. The characteristics of these fluctuations are summarized in Table 1.

The number of calculated time steps in the performed numerical simulations is typically 50 000, which corresponds to about 8 min of physical time. The numerical simulations show that after 15 000–20 000 time steps the LES solutions for all computed variables become

TABLE 1. Magnitudes of temperature ($\sigma_{T\text{in}}$, K) and velocity ($\sigma_{V\text{in}}$, m s^{-1}) fluctuations at the inlet for different test cases. The velocity rms values are the same for all three components. Level h symbolizes the elevation of temperature inversion at the inlet.

Case	$\sigma_{T\text{in}}$ below h	$\sigma_{T\text{in}}$ above h	$\sigma_{V\text{in}}$ below h	$\sigma_{V\text{in}}$ above h
ST	0	0	0	0
AT	50	50	0.3	0.3
VO	0	0	0.3	0.3
TO	50	50	0	0
BFC	50	0	0	0

statistically steady. The sections of time series between 20 001 and 50 000 time steps (approximately 5 min of physical time) are used for the calculation of statistics. In the wind tunnel CBL, the statistics are typically evaluated from the time series of about 2.5 min long, sampled with a resolution of 100 Hz. Based on numerical and experimental tests, these time series have been found to be long enough to provide consistent and reproducible turbulence statistics.

The statistics evaluated during each LES run are listed below. Note that the overbars in the following expressions of statistics denote the operation of time averaging (contrary to section 2, where overbars designate filtered variables), and the primes are the deviations from the time averages.

1) Means (time averages): $\overline{u}$, $\overline{v}$, $\overline{w}$, and $\overline{T}$.
2) Variances:
   $\overline{u'^2}$, $\overline{v'^2}$, $\overline{w'^2}$, and $\overline{T'^2}$ resolved;
   $\overline{u'^2}$, $\overline{v'^2}$, and $\overline{w'^2}$ total (resolved + subgrid):
   $\overline{u'^2} + 2E/3$, $\overline{v'^2} + 2E/3$, and $\overline{w'^2} + 2E/3$.
3) Third-order moments: $\overline{w'^3}$ and $\overline{T'^3}$.
4) Components of the vertical turbulent flux of momentum:
   $\overline{w'u'}$ and $\overline{w'v'}$ resolved;
   $\overline{w'u'}$ and $\overline{w'v'}$ total (resolved + subgrid):
   $\overline{w'u' - K_m(\partial u/\partial z + \partial w/\partial x)}$ and
   $\overline{w'v' - K_m(\partial v/\partial z + \partial w/\partial y)}$.
5) Vertical component of the turbulent kinematic heat (temperature) flux:
   $\overline{w'T'}$ resolved;
   $\overline{w'T'}$ total (resolved + subgrid): $\overline{w'T' - K_h \partial T/\partial z}$.

b. Evolution of temperature field and convective mixing in the wind tunnel

Let us first consider the development of temperature field in the basic configuration of the wind tunnel flow. The flow temperature in the tunnel is measured at five fixed locations corresponding to positions of windows used for the laser Doppler velocity measurements. The windows are located at $x = 0.68$ m (window 1), $x = 2.33$ m (window 2), $x = 3.98$ m (window 3), $x = 5.63$ m (window 4), and $x = 7.28$ m (window 5). The observations of mean temperature profile in these windows are illustrated in Fig. 2.

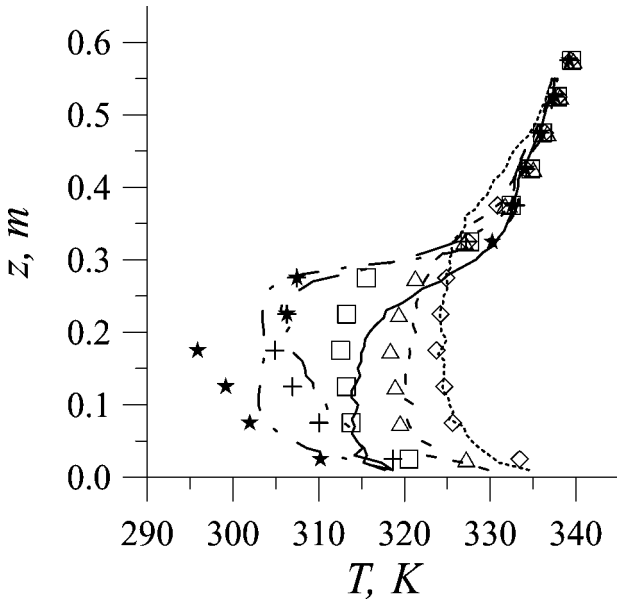

FIG. 2. Mean temperature profiles for the basic flow configuration. Lines show wind tunnel measurements, and symbols present the LES data for the BFC. Different line and marker styles correspond to different locations in the simulation domain: dashed–dotted lines and stars to $x = 0.68$ m; dashed–double-dotted lines and crosses to $x = 2.33$ m; solid lines and squares to $x = 3.98$ m; dashed lines and triangles to $x = 5.63$ m; and dotted lines and rhombuses to $x = 7.28$ m.

At the first location, $x = 0.68$ m, the shape of temperature profile is quite similar to that of the inlet profile schematically shown in Fig. 1. Heated, unstably stratified air near the surface occupies roughly one-third of the depth of the initially neutral layer. The turbulent motions generated by buoyancy are not yet developed to mix up this near-surface air. The changes in the rest of the temperature field are not significant.

Downwind of the first location, the depth of the zone warmed by convective heat transfer from the surface increases. At $x = 2.33$ m, only the uppermost portion of the initially neutral layer retains its original temperature, and the beginning of the inversion erosion can be pointed out in the temperature profile. The overall temperature lapse rate below the inversion is smaller than at $x = 0.68$ m due to the stronger turbulent mixing. Nevertheless, at this stage of flow evolution the convective turbulence is still not strong enough to mix up the whole below-inversion region.

Between $x = 2.33$ and $x = 3.98$ m the temperature profile changes its shape. The kneelike profile below the inversion at $x = 2.33$ m is replaced by the relatively straight profile at $x = 3.98$ m. The latter shape is characteristic of the temperature profile in the convectively mixed layer that is well known from atmospheric observations of convection; see, for instance, Lenschow (1998).

Based on these observations we conclude that the unstable premixed layer transforms into the convectively mixed layer over a comparatively short fetch range and apparently in a nonequilibrium way as was noticed by Fedorovich and Kaiser (1998). In the following we will refer to this transformation as transition.

In our opinion, the transition occurs as follows. Insufficient mixing at the early stages of convection leads to accumulation of potential energy in the unstable two-layer fluid system composed of a hot layer underlying a pool of cooler and less buoyant air. This unstable system eventually overturns and the accumulated energy is transformed into kinetic energy of turbulent fluctuations that effectively mix up the underinversion air. We will discuss below the variations of turbulence structure associated with the transition.

Downstream of the transition region, at $x = 5.63$ and $x = 7.28$ m, the mean flow temperature profile retains the characteristic CBL shape. We find a sharp drop of temperature in the near-surface layer, an approximately uniform temperature distribution in the mixed layer, an increase of T with height across the inversion, and an undisturbed thermal regime in the stably stratified flow above the inversion.

c. *LES of transition regimes with different inflow conditions*

Let us now consider which inlet conditions in the LES provide the best match for the observed turbulence regime in the wind tunnel CBL. These conditions should reproduce the actual conditions at the test section inlet. However, it is very difficult, not to say impossible, to measure turbulence directly at the inlet. Because of that, a series of special measurements have been performed in the first window, at $x = 0.68$ m, in order to estimate the fluctuations of flow parameters over the inlet plane. It has been found that substantial temperature and velocity fluctuations are typically present in the two lower layers of the tunnel that are operated in the open-circuit regime. Depending on the conditions in the ambient air, the temperature fluctuations in these lower layers may reach several degrees kelvin, and the velocity fluctuations may be of the order of 0.1 m s^{-1}. Above the inversion, inside the layers operated in the closed-circuit regime, the rms values of the temperature and velocity fluctuations are about one order of magnitude smaller than below the inversion.

These estimates have been used for setting the nonstationary components of the inlet velocity and temperature fields in the LES experiments (see section 2). In the following sections we will consider the results of LES runs with various choices for the inlet conditions. Our aim is to identify the best LES match for the basic wind tunnel CBL case described in Fedorovich et al. (1996).

1) STATIONARY INFLOW WITHOUT DISTURBANCES (CASE ST)

First we present the LES results corresponding to the stationary inflow with no resolved-scale velocity and temperature fluctuations (the ST case in Table 1). The LES results presented in Fig. 3 show that with such inflow conditions the transition to the well-mixed CBL occurs within the 5–7-m distance range from the inlet. This numerical prediction contradicts the experimental data in Fig. 2 that indicate that the wind tunnel flow becomes convectively mixed much earlier, at $x < 4$ m (see also the turbulence evolution patterns in Fedorovich and Kaiser 1998). Thus, in the numerically simulated flow without initial disturbances, the turbulence and mixing below the inversion develop much more slowly than in the wind tunnel CBL. Such insufficient mixing leads to a substantial accumulation of potential energy in the aforementioned unstable two-layer fluid system that precedes the transition. The eventual release of energy in the transition zone has a form of turbulence outbreak that is clearly seen in the patterns of all LES turbulence statistics shown in Fig. 3. The values of kinematic heat flux inside the transition region considerably exceed its constant input value of 1 K m s^{-1}, which indicates the nonequilibrium character of the observed transition. One may also notice that the regions of maximum values of upward heat flux and downward entrainment flux are not horizontally collocated. The entrainment essentially occurs at the downwind side of the turbulence bubble caused by the energy release. Downwind of the transition region, the vertical extension of convectively mixed zone does not change significantly with distance, and turbulence levels within this zone return to smaller values than in the transition region.

2) FLOW WITH TEMPERATURE AND VELOCITY DISTURBANCES ALL OVER THE INLET (CASE AT)

Next we consider the opposite case when the random temperature and velocity disturbances are prescribed over the entire inlet plane [the all together disturbance (AT) case in Table 1]. In this case (see Fig. 4), the disturbances affect the flow portions below and above the imposed inversion in a different way.

At $z < 0.3$ m, the premixing caused by initial fluctuations intensifies turbulent exchange and provides faster transition to the convectively mixed stage than in the case of stationary inflow (cf. flow evolution patterns in Figs. 3 and 4). Furthermore, this transition happens in a much more gradual way than in the latter case because energy accumulation below the inversion in the pretransition stage is not very significant. As a result, the entrainment associated with the transition is comparatively weak and the convectively mixed layer after the transition is not as thick as in the stationary inflow case. Due to advection, the temperature variance maximum in the inversion layer is shifted downwind with

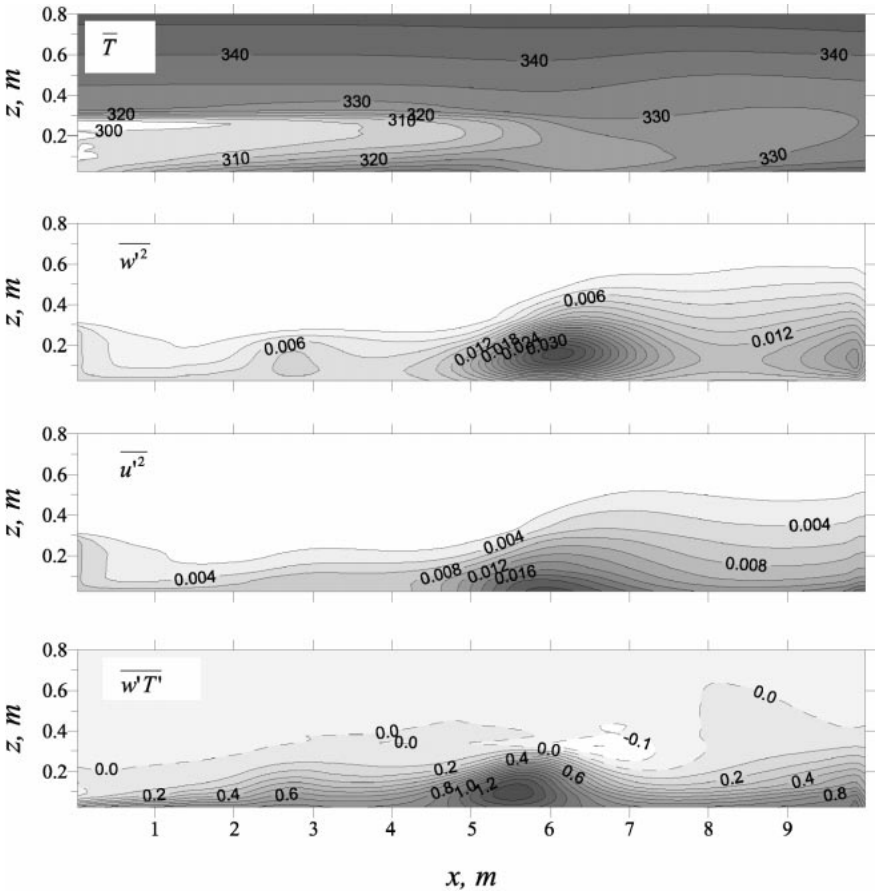

FIG. 3. Simulated distributions of mean temperature and turbulence statistics (total values) in the central plane of domain with stationary inflow conditions (case ST). Temperature is given in K, velocity variances in $m^2\ s^{-2}$, and heat flux in K m s^{-1}.

respect to the region of enhanced temperature fluctuations close to the floor. Earlier we have noted a similar shift in the pattern of kinematic heat flux (the lowest plot in Fig. 3).

The disturbances above $z = 0.3$ m lead to the formation of a layered structure in the initially linearly stratified flow region. In the temperature field, a steplike structure is formed within a 2-m-long adjustment region downwind of the inlet and this structure is preserved throughout the rest of the domain. The resulting temperature field is composed of relatively thick layers with almost constant temperature (quasi-mixed layers) separated by thin layers with jumplike temperature changes. The temperature fluctuations are confined to these interfacial layers, whereas the zones with enhanced velocity fluctuations are located within the quasi-mixed layers. These temperature and velocity fluctuations die out fast with distance as a result of damping by the stable stratification. A similar layered structure of the density field in a decaying turbulence has been observed in the laboratory experiments of Pearson and Linden (1983).

3) FLOWS WITH VELOCITY OR TEMPERATURE DISTURBANCES ALL OVER THE INLET (CASES VO/TO)

Simulation results for the velocity disturbances only (VO) and temperature disturbances only (TO) cases (not shown, but the parameters of these cases are given in Table 1) have been found to lie in between the results for the ST and AT cases. Turbulence statistics for the VO case show similar behavior to their ST counterparts except for a short range close to the inlet, where a slight enhancement of velocity variances due to initial flow disturbances is observed. In the absence of temperature fluctuations these disturbances do not produce any significant mixing effect and the delay in the transition is almost as long as in the ST case.

The TO case turns out to be close to the AT case with respect to observed features of the turbulence structure below the inversion. Above the inversion, the TO case velocity variances are noticeably smaller than in the AT case. Nevertheless, the layered structure of the temperature field in the stably stratified region is observed

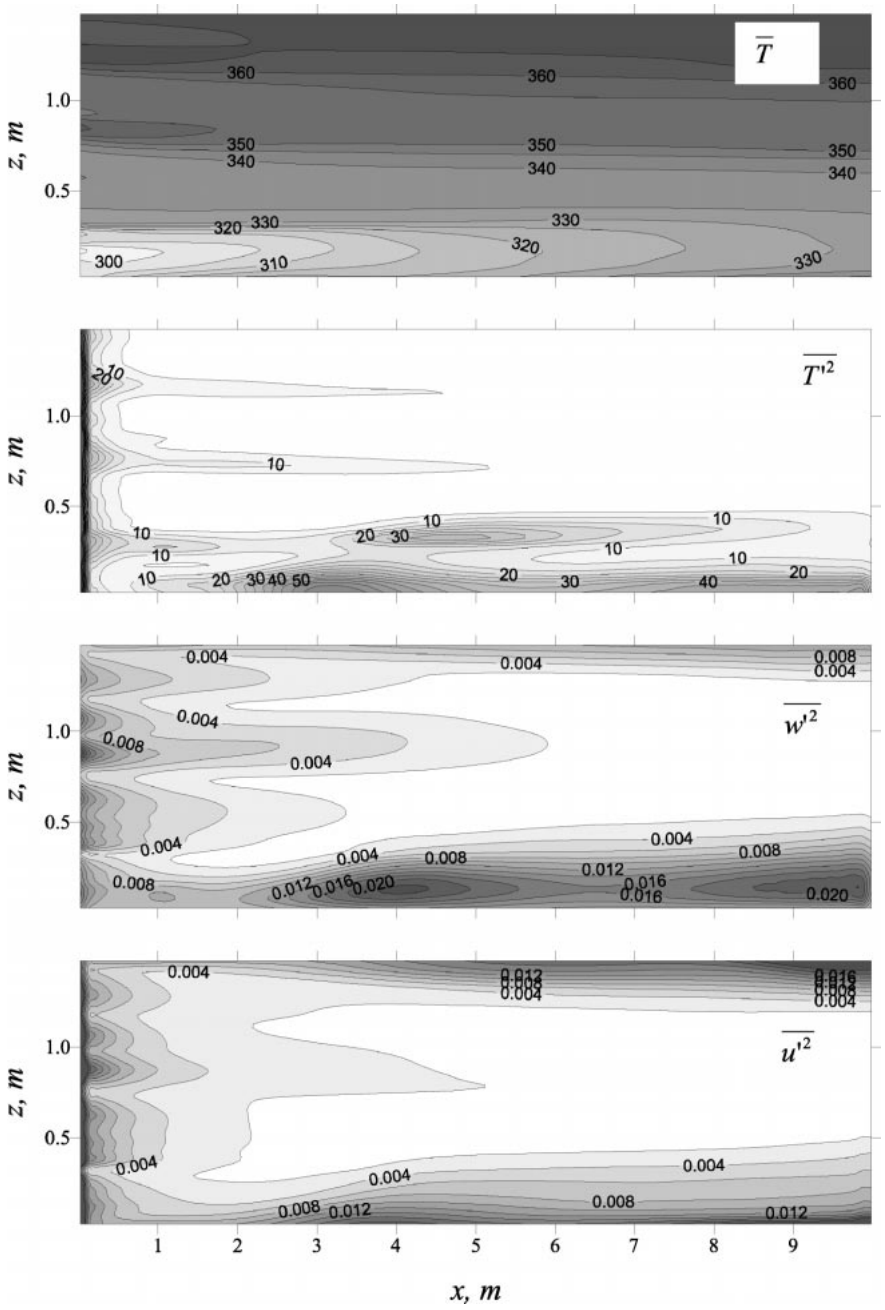

FIG. 4. Simulated distributions of mean temperature and turbulence statistics (total values) in the central plane of the domain with random temperature and velocity fluctuations generated in all nodes of the inlet plane (case AT). Temperature is given in K, temperature variance in K^2, and velocity variances in $m^2\ s^{-2}$.

again in the TO case. It looks quite similar to the steplike temperature pattern in the AT case.

4) INFLOW WITH TEMPERATURE DISTURBANCES BELOW THE INVERSION (BFC)

Finally we consider LES results for the basic flow case (BFC), when only the lowest 0.3-m-deep portion of the inlet temperature field has prescribed random disturbances (see Table 1). The evolution of turbulence regime below the inversion in this case (see Fig. 5) is very similar to the AT case, where in addition to the temperature disturbances velocity fluctuations are also present at the inlet. This suggests that transition processes in the simulated flow fields are mainly controlled by temperature inhomogeneities. Location of the tran-

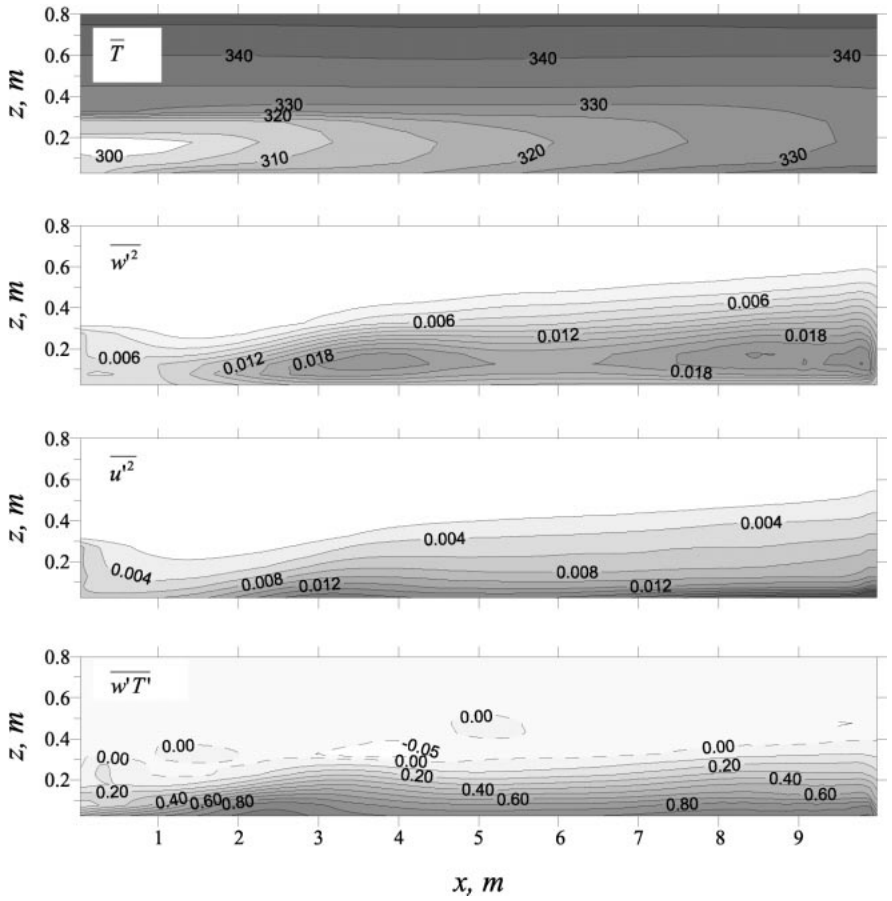

FIG. 5. Simulated distributions of mean temperature and turbulence statistics (total values) in the central plane of domain with random temperature fluctuations generated in the two lower layers of the incoming flow (BFC). Temperature is given in K, velocity variances in $m^2\ s^{-2}$, and heat flux in K m s^{-1}.

sition zone associated with the energy release and enhanced turbulence is now much closer to the position observed in the tunnel ($x \approx 3.5$ m) than in the ST case.

A comparison between temperature evolution patterns in the BFC and in the basic wind tunnel flow configuration is presented in Fig. 2. The LES results agree fairly with the wind tunnel data at $x = 3.98$ m (lee region of the transition zone), $x = 5.63$ and $x = 7.28$ m (quasi-homogeneous CBL). The LES and wind tunnel results decently conform also at $x = 2.33$ m, which is upstream of the transition region. At the first measurement location, $x = 0.68$ m, the agreement between the LES and wind tunnel data is not as good. This may be due to the insufficient resolution of LES in the near-inversion flow portion with huge temperature gradients at the pretransition stage of the CBL development.

Once the flow has passed the transition zone, the established convectively mixed layer with a quasi-uniform vertical temperature distribution slowly evolves downwind; see Fig. 5. The turbulence statistics show that the depth of the layer increases from approximately 0.35 m at the downstream side of transition region to 0.55 m at the domain outlet. As in the previously discussed cases, the entrainment maximum in the flow is observed at the lee side of transition region. Over the rest of the domain the entrainment heat flux is rather small. Such a small entrainment in the CBL after transition is in agreement with the wind tunnel results for the basic flow configuration discussed in Fedorovich et al. (1996) and Fedorovich and Kaiser (1998).

We conclude that the BFC seems to be the most relevant one to be investigated in relation to the wind tunnel results. It will be more comprehensively analyzed in section 4.

d. Resolved and subgrid contributions to simulated flow fields

The LES adequately reproduces the turbulent flow structure only in the case when energy carried by the large-scale resolved motions dominates the contribution to the total energy of the small-scale subgrid motions (Piomelli and Chasnov 1996). For the LES runs that have been carried out, the resolved and subgrid contri-

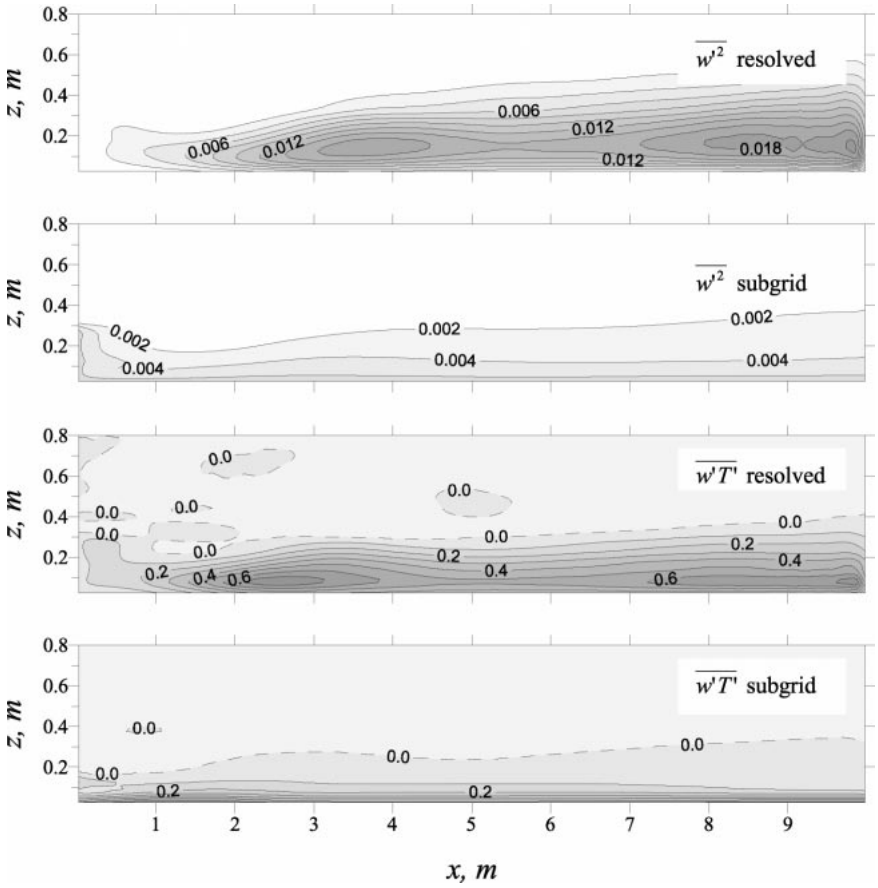

FIG. 6. Resolved and subgrid contributions to the vertical velocity variance and turbulent kinematic heat flux in the central plane of domain (BFC). Velocity variances are given in $m^2\ s^{-2}$ and heat flux in K m s^{-1}.

butions to different turbulence statistics have been evaluated separately. In Fig. 6, we show distributions of resolved and subgrid components of the vertical velocity variance and kinematic heat flux along the domain in the BFC.

In the main portion of the simulation domain, the resolved-scale contributions to both statistics are definitely larger than the subgrid ones. Within the transition region and throughout the quasi-homogeneous CBL that develops downwind, the contributions by resolved flow components are clearly dominant. The major part of the negative entrainment flux at the downwind side of transition region is maintained by the resolved motions. Before the transition stage, at $x < 1$ m, the dominance of the resolved contributions is not as clear. The resolved-scale motions are not yet developed in this flow region (this is especially noticeable in the $\overline{w'^2}$ pattern), and a substantial part of turbulence exchange occurs on the subgrid-scale level.

4. Turbulence structure in the basic flow case

Important information concerning the structure of turbulence at different stages of the CBL development can be obtained from the joint analysis of the numerically simulated turbulence fields and flow patterns visualized in the wind tunnel CBL. Visualization of the turbulence structure in the wind tunnel flow has been realized by means of the laser light sheet technique as described in Fedorovich et al. (1996) and Fedorovich and Kaiser (1998). A neutrally buoyant fog of tracer particles illuminated by a laser beam is used to portray the turbulence pattern. Assuming that the turbulent motion is adequately represented by the moving fog particles, one may compare the computed instantaneous flow patterns with the laser sheet visualizations.

First we consider the instantaneous LES patterns of temperature and vertical velocity corresponding to the BFC. They are presented in Fig. 7. One may notice that at the stage of the nonmixed unstable layer ($x < 3.5$ m) the thermal plumes rising from the surface are small and relatively densely packed. A pool of the cooler air is clearly visible above the hot near-surface layer. Farther downstream, the sizes of bulb-shaped plumes increase. At the same time, the plumes get detached from each other and zones of cooler descending air (downdrafts) grow between them. The downdrafts are well

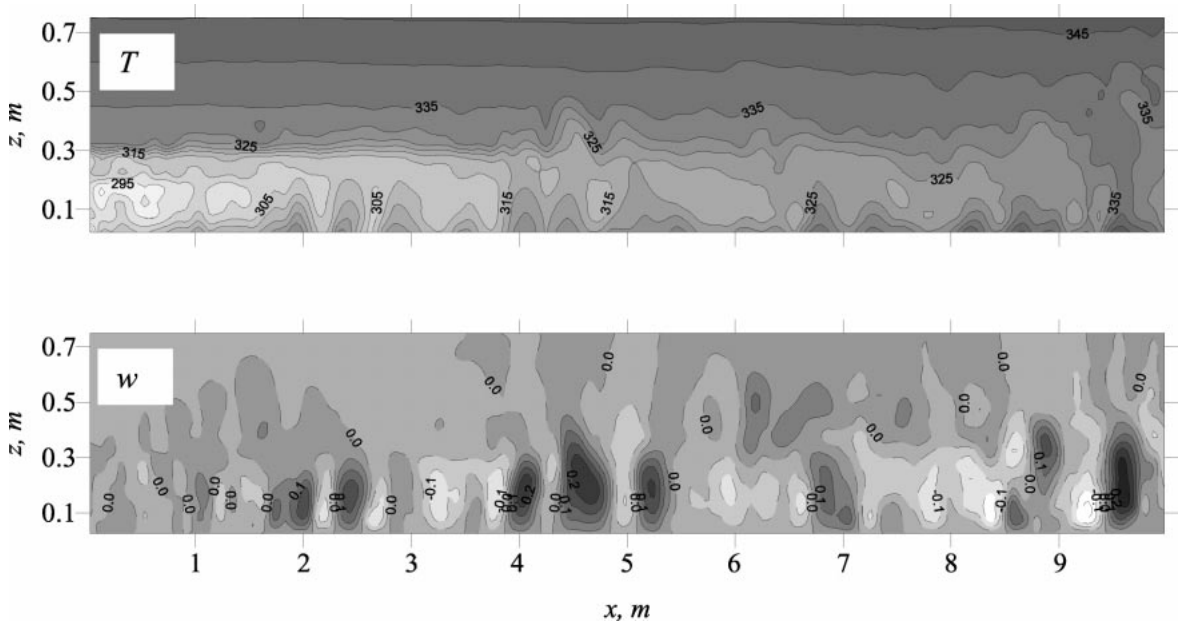

FIG. 7. Instantaneous temperature and vertical velocity distributions in the central plane of domain (BFC). Temperature is given in K and velocity in m s^{-1}.

displayed in the vertical velocity pattern. The horizontal scales of updrafts and downdrafts in the considered flow region are approximately the same. The temperature and velocity fields below the inversion are well correlated: the updrafts transport a warm air from the floor, while the compensating downdrafts carry cooler air. The capping inversion remains practically unaffected by these small-scale convective motions.

Within the range $3.5 < x < 5.5$ m the flow passes through the transition zone. Here, the release of potential energy accumulated in the unstable flow below the inversion initiates active upward and downward motions that provide the effective mixing of air below the inversion. In addition, these motions perturb the inversion and stimulate the entrainment of the warm air from above the inversion down into the convectively mixed layer. In the bulk of the layer, the main component of motion is directed upward, and the updrafts of hot air (in this stage they may be already qualified as convective thermals) dominate the narrower downdrafts. Closer to the top of the layer, in the entrainment zone, the downdrafts that transport warmer air downward are becoming wider at the expense of thermals, the horizontal dimensions of which decrease with height.

Downwind of the transition zone, the proportion between the dimensions of warm updrafts (thermals) and cool downdrafts is different compared to the pretransition flow phase. The flow pattern here consists of vast areas with relatively weak downward motions separated by the narrow and strong thermals that vertically pierce the whole layer. Such proportions between the areas of upward and downward motions are in good agreement with the atmospheric CBL observations presented in Lenschow and Stephens (1980) and Stull (1988). The velocity and temperature fields inside the main portion of the established CBL are still well correlated, but the temperature pattern at this stage is much less variable than the pattern in the pretransition region. The inversion in the posttransition phase looks quite convoluted and gets progressively weaker due to erosion caused by the rising thermals.

The next group of plots (Fig. 8) shows instantaneous temperature patterns derived from the LES in comparison with the wind tunnel flow visualizations. The uppermost pair of plots refers to the pretransition flow region (window 2, $x = 2.33$ m). The second pair of plots (window 3, $x = 3.98$ m) shows turbulence patterns within the transition region. Finally, the third pair (window 4, $x = 5.63$ m) refers to the stage of the fully developed convectively mixed layer.

Within the considered fetch range, the scales and geometry of convective elements undergo substantial changes. At the first location, the buoyant plumes in the unstable near-surface layer are rather small and only a few of them extend up to the capping inversion. In the wind tunnel visualization pattern, the peculiar, bubble- or fingerlike finescale convective elements can be observed at the top of the rising plumes. In the temperature pattern from the LES, the laterally elongated pools of cool nonmixed air are seen above the patchy blanket of hot air adjacent to the surface. The capping inversion in the pretransition stage is looking quite strong.

Further development of the turbulence structure in the tunnel is marked by the merging of plumes into the columnlike buoyant thermals, which are bigger and stronger than the plumes. The thermals and associated

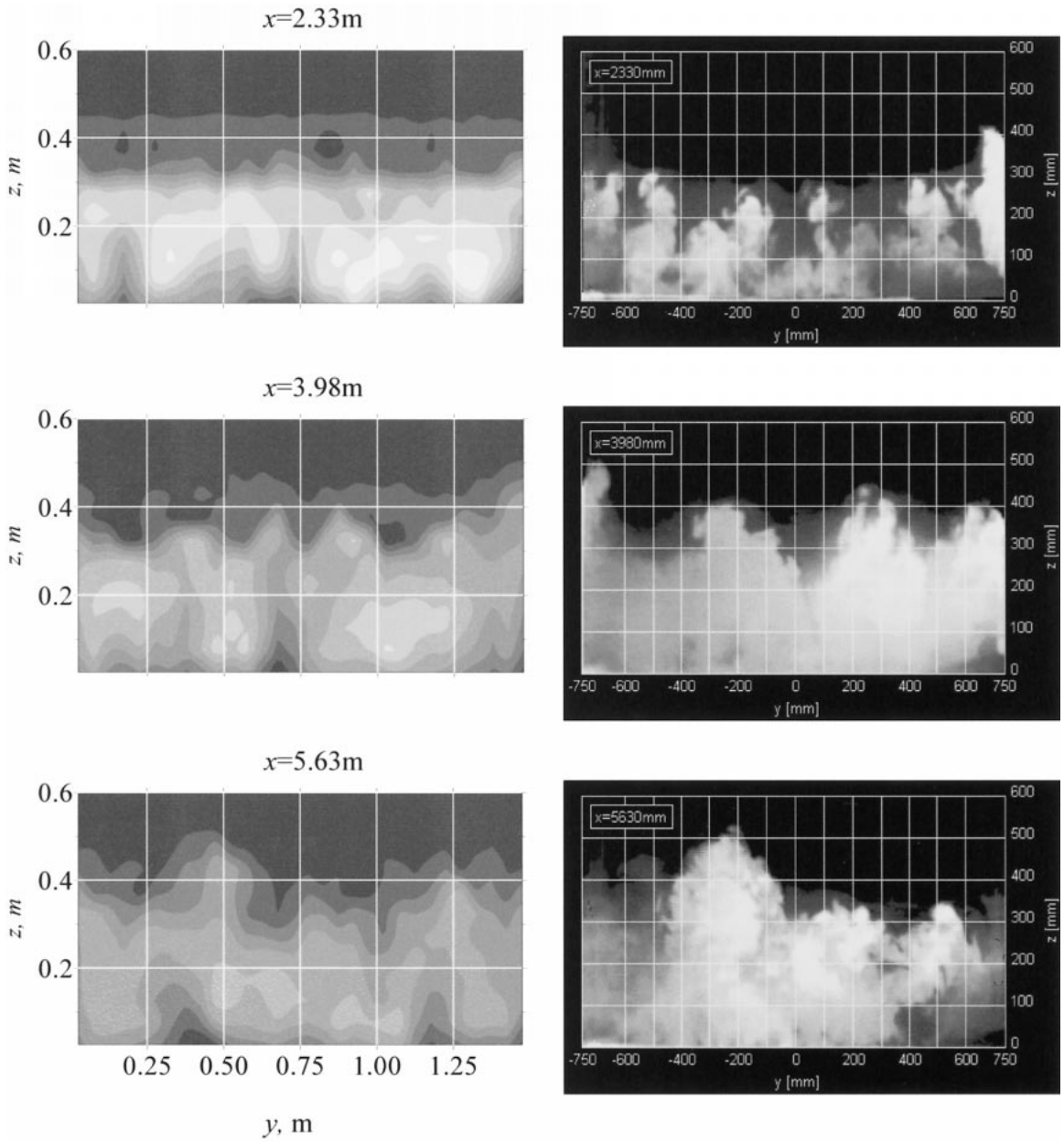

FIG. 8. Evolution of thermal structure in the BFC. Instantaneous temperature distributions calculated with the LES (left-hand field of the plot) are presented together with flow visualization patterns from the wind tunnel (right-hand field). Calculations and visualizations refer to three transverse cross sections located at different distances from the inlet.

cool downdrafts provide strong mixing in the transition region and effectively destroy the capping inversion. This is clearly illustrated in the LES pattern referring to the transition region ($x = 3.98$ m). Both LES and wind tunnel patterns display deep penetration of thermals in the stably stratified fluid above the inversion. The horizontal dimensions of thermals typically decrease with height, which is consistent with our previous observations (see Fig. 7) and with lidar images of thermals in the atmospheric CBL (Hooper and Eloranta 1986). It is remarkable that the tops of newborn thermals at $x = 3.98$ m are composed of the finescale buoyant elements looking like the ones atop the convective plumes in the pretransition region, at $x = 2.33$ m. These small-scale elements penetrate through the inversion ahead of the main body of the thermal.

The LES patterns do not possess a sufficient resolution to reproduce the aforementioned finescale elements. Nevertheless, one can notice that characteristic scales of the structures reproduced by the LES grow with x, whereas the small-scale structure elements disappear. Downwind of the transition region, at $x = 5.63$

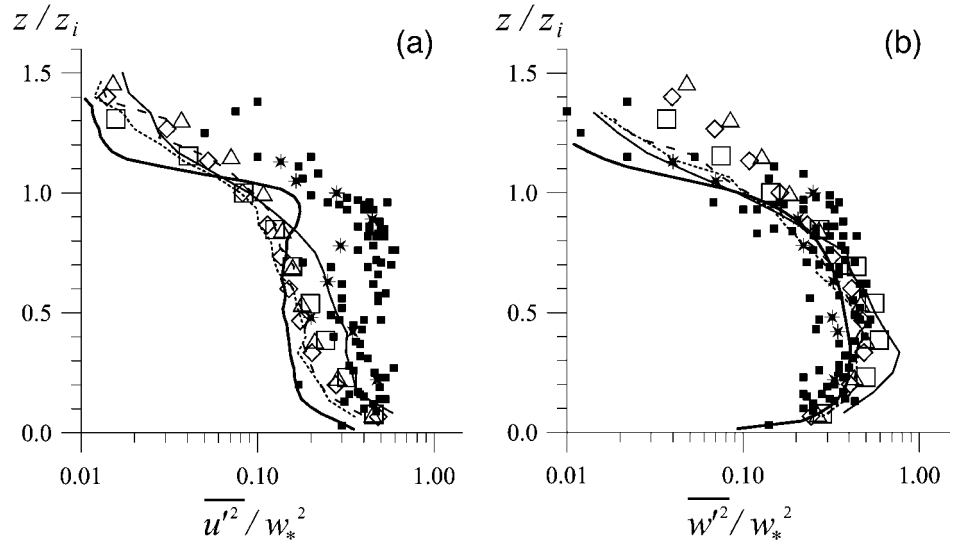

FIG. 9. Variances of the (a) longitudinal and (b) vertical velocity components from the present study (BFC, total values) in comparison with data from other CBL studies. The LES results for different locations along the domain are shown by markers: open squares correspond to $x = 3.98$ m, triangles to $x = 5.63$ m, and rhombuses to $x = 7.28$ m. The wind tunnel data for these locations are given by solid lines, dashed lines, and dotted lines, respectively. The LES results of Schmidt and Schumann (1989) for the shear-free CBL are shown by heavy solid lines, atmospheric measurements of Lenschow et al. (1980) and Caughey and Palmer (1979) by filled squares, and data from the Deardorff and Willis (1985) water tank model of the shear-free CBL by asterisks.

m, the thermal contours are becoming less ragged and the thermals are looking more dome-shaped than their counterparts in the transition stage. Such redistribution of scales in the temperature patterns obtained by the LES is consistent with the evolution of turbulence-scale structure in the wind tunnel CBL; see the two lower plots in Fig. 8.

Let us now proceed to a quantitative comparison of the LES results with corresponding wind tunnel data and with results coming from several other experimental and numerical studies of the CBL. The data employed for comparisons are obtained from various sources and from different cases of nonsteady, horizontally quasi-homogeneous CBL. It was shown in Fedorovich et al. (1996) and Fedorovich and Kaiser (1998) that the mean flow and turbulence characteristics measured in the post-transition region of the wind tunnel CBL compare fairly well with data from experimental and model studies of the slowly evolving nonsteady CBL.

Before they were plotted, the calculated turbulence characteristics had been normalized by the Deardorff (1970) convective scales, which are z_i for length, $w_* = (\beta Q_s z_i)^{1/3}$ for velocity, and $T_* = Q_s/w_*$ for temperature. Here, z_i is the mixed-layer depth, usually defined as elevation of the heat flux minimum within the entrainment zone; $\beta = g/T_0$ is the buoyancy parameter (see section 2); and Q_s is the surface value of the turbulent kinematic heat flux. Despite the well-known shortcomings of the mixed-layer scaling (Wyngaard 1992), it has been used for decades as convenient framework for comparison of measurements from different CBL experiments and for verification of numerical simulations of the CBL.

The influence of transition on the velocity variances in the simulated CBL is demonstrated in Fig. 9. At $x = 3.98$ m (which lies within the transition zone), both variances are obviously larger than at the two subsequent locations downwind of the transition region. The agreement between the LES and wind tunnel data at $x = 5.63$ and $x = 7.28$ m is very good. Such an agreement is rather unusual for the horizontal velocity variance (Fig. 9a) because this parameter is known to be quite poorly reproduced by LES of the CBL [see Nieuwstadt et al. (1993), and note the large divergence of data from other sources in Fig. 9a]. At $x = 3.98$ m, the agreement of LES predictions with wind tunnel measurements is not as good.

With respect to the other data shown in Fig. 9 we note the following. Compared to the pure shear-free CBL, which was numerically simulated by Schmidt and Schumann (1989), the larger $\overline{u'^2}$ values at small z are caused in our case by the additional turbulence production in the lower CBL portion due to surface shear (Fedorovich et al. 1996). The water tank model and atmospheric measurements both provide rather large values of $\overline{u'^2}$ over the whole CBL depth. In the water tank, this is presumably due to the horizontal variations of heat flux across the bottom of the tank (Schmidt and Schumann 1989). Mesoscale disturbances of the wind field affecting the local turbulence regime in the CBL may be used as an explanation for the larger atmospheric $\overline{u'^2}$ values (Kaiser and Fedorovich 1998).

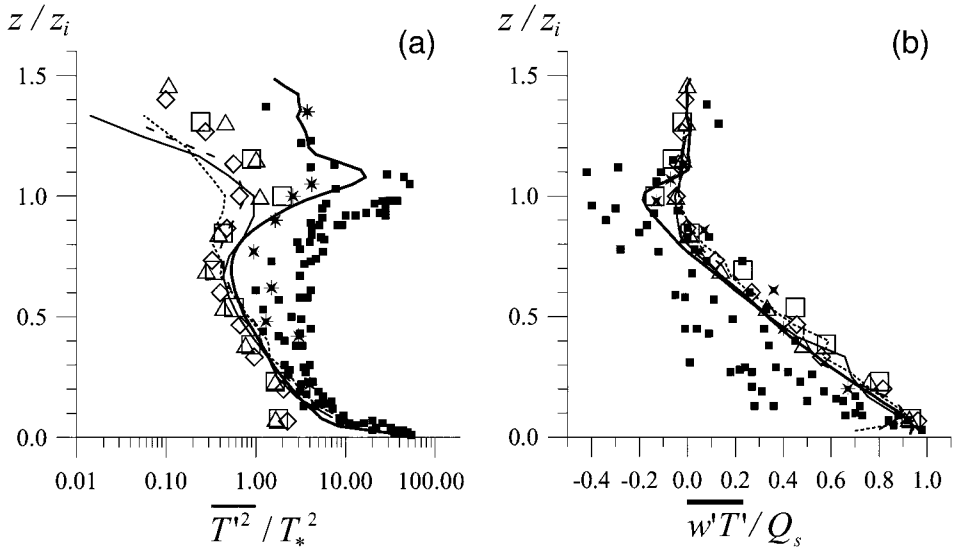

FIG. 10. (a) Temperature variance and (b, total values) vertical kinematic heat flux from the present study (BFC) in comparison with data from other CBL studies. Notation is the same as in Fig. 9. Atmospheric measurements (filled squares) are represented by data from Caughey and Palmer (1979).

Within the entrainment region near the CBL top (z/z_i of the order of 1), two main mechanisms can be responsible for the enhancement of horizontal velocity fluctuations. The first one is a sideward transport of air from the thermals decelerated by the inversion layer and the second one is an elevated wind shear (its effect on the CBL turbulence regime is discussed in Fedorovich et al. 2001). The latter mechanism is likely to be one of the reasons for the enlarged variances of u in the upper part of the atmospheric CBL. The destruction of rising thermals by comparatively strong capping inversions in the cases of shear-free CBL has been reproduced numerically by Schmidt and Schumann (1989) and in the water tank by Deardorff and Willis (1985). Such destruction results in a clear $\overline{u'^2}$ maximum located at approximately $z/z_i = 1$. Our numerical and laboratory results for the CBL with a weaker capping inversion give at most a change (bend) of the slope in the $\overline{u'^2}$ profile at this level.

The vertical velocity variance in the CBL is less affected by the nonbuoyant forcing than $\overline{u'^2}$ (Kaiser and Fedorovich 1998). This may be a reason for relatively small scatter of $\overline{w'^2}$ values from different datasets represented in Fig. 9b. Downstream of the transition zone, our numerical and wind tunnel data show larger values of $\overline{w'^2}$ compared to the data from other sources. This must be due to the effect of the transition zone. Before the numerical simulation has been performed, such enhancement of velocity variances in the wind tunnel CBL seemed inconsistent with other observations (Fedorovich et al. 1996). Thus, the complement of the wind tunnel experiments by numerical simulations has been rather helpful in analyzing the consistency of the observations and understanding the mechanisms that determine the CBL turbulence structure.

The effects of transition can be identified also in the simulated and measured temperature variance and kinematic heat flux profiles (Fig. 10). The temperature variance inside the entrainment zone is considerably larger in the transition region ($x = 3.98$ m) than throughout the quasi-homogeneous CBL downwind. This is also the case of temperature flux caused by entrainment in the transition zone and at the downwind locations, $x = 5.63$ and $x = 7.28$ m. The larger values of both quantities in the transition zone are apparently due to the turbulence enhancement associated with transition. At $x = 3.98$ m, the relatively big temperature increment across the inversion (see Fig. 2) contributes to the enlargement of temperature fluctuations in addition to the effect of transition. In the main portion of the CBL, the temperature variance and heat flux profiles from the LES and wind tunnel experiments practically coincide for all locations.

The LES and wind tunnel data shown in Fig. 10 seem to diverge near the surface, at $z/z_i < 0.2$. In the case of temperature variance, this divergence may be caused by poor reproduction of the near-surface temperature fluctuations in the employed LES procedure, which does not explicitly account for the subgrid component of $\overline{T'^2}$. The near-surface drop of the heat flux in the wind tunnel case can be explained by the insufficient development of turbulence near the wind tunnel floor and by certain measurement problems discussed in Fedorovich et al. (1996).

The temperature variances presented in Fig. 10a explicitly show the effects of inversion strength and outer flow stability on the magnitude of temperature fluctuations at the CBL top. The $\overline{T'^2}$ values from the present study (the case of relatively weak capping inversion) are the smallest at $z/z_i = 1$, while the water tank and

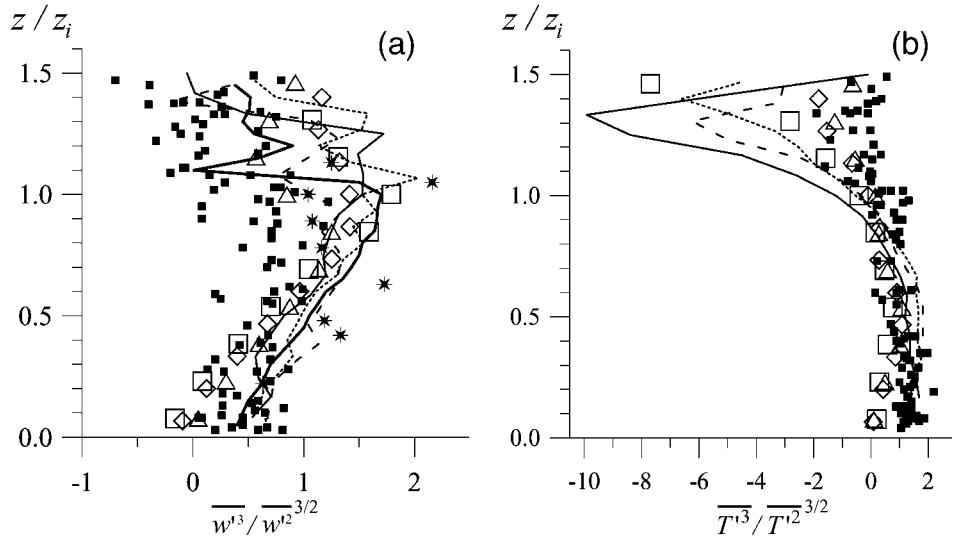

FIG. 11. Skewness of (a) the resolved-scale vertical velocity and (b) temperature fluctuations from the present study (BFC) in comparison with data from other CBL studies. Notation is the same as in Fig. 9. Atmospheric measurements (filled squares) are represented by data from Sorbjan (1991).

LES simulations of shear-free CBL with stronger temperature gradients across the inversion and above it provide roughly 10 times higher values of $\overline{T'^2}$ at the same dimensionless height.

The atmospheric data on $\overline{w'T'}$ in Fig. 10b are strongly scattered and deviate noticeably from the linear profile. This is probably a result of contributions to the heat balance of atmospheric CBL by a variety of nonconvective driving mechanisms (Fedorovich et al. 1996). In the main portion of CBL, at $z/z_i < 0.9$, our laboratory and numerical data agree well with the $\overline{w'T'}$ values from the LES and water tank studies of the shear-free CBL. Inside the entrainment zone, however, the magnitude of the heat flux in the CBL from the present study is much smaller than in the CBL cases with stronger capping inversions.

Profiles of the skewness of the vertical velocity and temperature fluctuations are shown in Fig. 11. The skewness of the vertical velocity fluctuations (Fig. 11a) is positive in the main portion of CBL. This reflects a characteristic feature of the turbulent convection structure, which is composed of narrow, fast thermals and broad, slow downdrafts. The vertical velocity skewness derived from the atmospheric measurements is quite uniform in the vertical. Such uniformity points to a more homogeneous structure of up- and downdrafts in the atmosphere compared to the CBL cases reproduced numerically and in the laboratory. The comparatively small values of the w skewness predicted by LES at small z apparently result from insufficient resolution of employed LES procedure in the near-surface region of the CBL, where the subgrid effects play an important role (see also Fig. 5).

The distribution of the w skewness at $z/z_i > 1$ in Fig. 11a shows that at the top of atmospheric CBL the upward component of turbulent motion (positive w') is in an approximate balance with the downward component (negative w'). At the same time, the vertical velocities in the upper portion of wind tunnel CBL are persistently skewed positively. In this case, the upward component of w is maintained by compact and active buoyant elements, while the downward component w is associated with the thermally nearly neutral and slowly descending air particles, which contribute only slightly to the net transport of heat across the inversion (see T skewness in Fig. 11b). As we have already seen in Fig. 10b, the resulting heat flux of entrainment in this case is rather small.

Temperature skewness shown in Fig. 11b reaches its maximum approximately in the middle of the convectively mixed layer, where the simulation results agree fairly well with the atmospheric data. Close to the surface, the skewness values predicted by the LES are markedly smaller than their wind tunnel counterparts. As in the case of vertical velocity skewness, this may be an indication of the inadequate performance of LES in the near-surface sublayer. Above the middle portion of CBL, the computed skewness slowly decays with height toward $z/z_i = 1$, which is in good agreement with the atmospheric results.

The temperature skewness data diverge drastically in the upper part of the CBL. This is one more manifestation of difference between regimes of entrainment in the wind tunnel CBL and in the atmospheric CBL. In the former case, the interaction of relatively narrow and cool thermals with a weak capping inversion leads to very negatively skewed temperature distribution close to the CBL top. The earlier discussed buoyant fingerlike elements rising from the tops of thermals in the wind tunnel CBL (see visualization patterns in Fig. 8) may

additionally contribute to the enlargement of temperature skewness in the entrainment zone. The thermals in the atmospheric CBL with presumably stronger capping inversion are squashed and effectively destroyed by stable density stratification in the inversion layer. This results in the less skewed temperature distribution at the top of the atmospheric CBL.

5. Summary and conclusions

We have considered the evolution of turbulence structure in a horizontally developing sheared convective boundary layer (CBL) capped by a weak temperature inversion and with a moderate stability in the turbulence-free flow above the CBL. A combination of numerical technique (LES) and wind tunnel experiments has been applied to study the development of this boundary layer. Such combination has provided an opportunity to investigate a number of CBL flow regimes, which had not been reproduced previously either numerically or in the laboratory. It has turned out to be helpful also for understanding some experimentally observed but not sufficiently explained CBL turbulence features.

The development of the studied CBL occurs in three stages. In the initial stage, the turbulent convection is not yet fully developed. Next a transition occurs that is associated with turbulence generation caused by the release of potential energy accumulated during the initial stage. After the transition, the boundary layer develops into a quasi-homogeneous convectively mixed layer. Location of the transition region and the corresponding change in turbulence regime are strongly dependent on the magnitude and distribution of disturbances in the flow at the inlet. The CBL evolution in the pretransition stage is primarily controlled by the temperature fluctuations in the incoming flow. The influence of velocity fluctuations at this stage is subordinate to the effect of the temperature inhomogeneities. In the case of no inlet disturbances, the turbulent mixing forced by heat transfer from the surface develops rather slowly and a substantial accumulation of the potential energy takes place during the pretransition stage in the unstable two-layer fluid system capped by inversion. The release of this energy is accompanied by a dramatic enhancement of turbulence in the comparatively narrow bubble-shaped transition zone. With the temperature fluctuations introduced at the inlet, the pretransition phase is much shorter, and the turbulence enhancement in the transition region is less pronounced.

Maximum values of the upward heat flux are observed inside the transition zone while the flow region with most intensive entrainment heat flux is slightly shifted downstream of the transition zone. An analogous horizontal shift is observed in the temperature variance pattern, where the elevated region with strong temperature fluctuations in the inversion layer is displaced downwind with respect to the temperature variance maximum associated within the transition. In the flow section downwind of the transition zone, turbulence levels are considerably lower than inside the zone, and the turbulence pattern is characterized by a comparatively weak horizontal variability.

In the numerically simulated flow case with random temperature and velocity disturbances prescribed in all nodes of the inlet plane, a peculiar layered structure is formed in the linearly stratified fluid above the inversion. The corresponding temperature pattern above the inversion is built up of relatively thick quasi-mixed layers of constant temperature separated by thin interfacial layers associated with jumplike temperature changes. Zones of the enlarged temperature fluctuations are confined to these interfacial layers, whereas the regions with enhanced velocity fluctuations are located within the quasi-mixed layers.

The numerically simulated CBL case with only temperature fluctuations generated in the lower portion of the inlet plane has been found to be the best match for the basic CBL flow configuration reproduced in the wind tunnel. The second-order turbulence moments derived from the LES for this case show good agreement with the wind tunnel measurements. The main features of transition, including the turbulence enhancement within the transition zone, are successfully captured by the LES.

The combined numerical and wind tunnel investigation has demonstrated that in the CBL beyond the transition region the turbulence is noticeably skewed throughout the whole layer. In the entrainment zone, the temperature is strongly negatively skewed; meanwhile the vertical velocity skewness keeps positive values up to the very top of the CBL. Smaller-scale secondary buoyant elements have been identified at the tops of larger-scale buoyant plumes and thermals penetrating through the capping inversion. The magnitudes of velocity and temperature skewness in the entrainment region of the simulated CBL are found to be larger than corresponding magnitudes in the upper portion of atmospheric CBL. It is suggested that small values of the entrainment heat flux in the simulated CBL are associated with the above-specified structural properties of turbulence in the CBL capped by weak inversion.

Acknowledgments. Financial support provided for the study by the Deutsche Forschungsgemeinschaft (DFG) within the Project ''Untersuchung and Parametrisierung der Wechselwirkungen von Skalen der Turbulenz konvektiver Grenzschichtströmungen unter Verwendung einer einheitlichen Datengrundlage aus Naturmessungen, Windkanalversuchen und numerischen Modellen'' is gratefully acknowledged.

REFERENCES

Caughey, S. J., and S. G. Palmer, 1979: Some aspects of turbulence structure through the depth of the convective boundary layer. *Quart. J. Roy. Meteor. Soc.*, **105,** 811–827.

Deardorff, J. W., 1970: Convective velocity and temperature scales for the unstable planetary boundary layer and for Raleigh convection. *J. Atmos. Sci.,* **27,** 1211–1213.

——, 1972: Numerical investigation of neutral and unstable planetary boundary layers. *J. Atmos. Sci.,* **29,** 91–115.

——, 1980: Stratocumulus-capped mixed layers derived from a three-dimensional model. *Bound.-Layer Meteor.,* **18,** 495–527.

——, and G. E. Willis, 1985: Further results from a laboratory model of the convective planetary boundary layer. *Bound.-Layer Meteor.,* **32,** 205–236.

Fedorovich, E., and R. Kaiser, 1998: Wind tunnel model study of turbulence regime in the atmospheric convective boundary layer. *Buoyant Convection in Geophysical Flows,* E. J. Plate et al., Eds., Kluwer, 327–370.

——, ——, M. Rau, and E. Plate, 1996: Wind-tunnel study of turbulent flow structure in the convective boundary layer capped by a temperature inversion. *J. Atmos. Sci.,* **53,** 1273–1289.

——, F. T. M. Nieuwstadt, and R. Kaiser, 2001: Numerical and laboratory study of horizontally evolving convective boundary layer. Part II: Effects of elevated wind shear and surface roughness. *J. Atmos. Sci.,* in press.

Hooper, W. P., and E. W. Eloranta, 1986: Lidar measurements of wind in the planetary boundary layer: The method, accuracy and results from joint measurements with radiosonde and kytoon. *J. Climate Appl. Meteor.,* **25,** 990–1001.

Kaiser, R., and E. Fedorovich, 1998: Turbulence spectra and dissipation rates in a wind tunnel model of the atmospheric convective boundary layer. *J. Atmos. Sci.,* **55,** 580–594.

Lenschow, D. H., 1998: Observations of clear and cloud-capped convective boundary layers, and techniques for probing them. *Buoyant Convection in Geophysical Flows,* E. J. Plate et al., Eds., Kluwer, 185–206.

——, and P. L. Stephens, 1980: The role of thermals in the convective boundary layer. *Bound.-Layer Meteor.,* **19,** 509–532.

——, J. C. Wyngaard, and W. T. Pennel, 1980: Mean-field and second-moment budgets in a baroclinic, convective boundary layer. *J. Atmos. Sci.,* **37,** 1313–1326.

Mason, P. J., 1989: Large-eddy simulation of the convective atmospheric boundary layer. *J. Atmos. Sci.,* **46,** 1492–1516.

Moeng, C.-H., 1984: A large-eddy simulation for the study of planetary boundary layer turbulence. *J. Atmos. Sci.,* **41,** 2052–2062.

Nieuwstadt, F. T. M., 1990: Direct and large-eddy simulation of free convection. *Proc. Ninth Int. Heat Transfer Conf.,* Jerusalem, Israel, American Society of Mechanical Engineering, 37–47.

——, and R. A. Brost, 1986: Decay of convective turbulence. *J. Atmos. Sci.,* **43,** 532–546.

——, P. J. Mason, C.-H. Moeng, and U. Schumann, 1993: Large-eddy simulation of the convective boundary layer: A comparison of four computer codes. *Turbulent Shear Flows 8,* F. Friedrich et al., Eds., Springer-Verlag, 343–367.

Ohya, Y., and T. Uchida, 1999: Wind tunnel study and DNS of stable boundary layers and convective boundary layers in the atmosphere. *Turbulence and Shear Flow Phenomena—1,* S. Banerjee and J. K. Eaton, Eds., Begell House, 589–594.

——, K. Hayashi, S. Mitsue, and K. Managi, 1998: Wind tunnel study of convective boundary layer capped by a strong inversion. *J. Wind Eng.,* **75,** 25–30.

Pearson, H. J., and P. F. Linden, 1983: The final stage of decay of turbulence in stably stratified fluid. *J. Fluid Mech.,* **134,** 195–203.

Piomelli, U., and J. R. Chasnov, 1996: Large-eddy simulations: Theory and applications. *Turbulence and Transition Modelling,* M. Hallbäck et al., Eds., Kluwer, 269–336.

Rau, M., and E. J. Plate, 1995: Wind tunnel modelling of convective boundary layers. *Wind Climate in Cities,* J. E. Ermak et al., Eds., Kluwer, 431–456.

Schmidt, H., and U. Schumann, 1989: Coherent structure of the convective boundary layer derived from large-eddy simulations. *J. Fluid. Mech.,* **200,** 511–562.

Sorbjan, Z., 1991: Evaluation of local similarity functions in the convective boundary layer. *J. Appl. Meteor.,* **30,** 1565–1583.

Stull, R. B., 1988: *An Introduction to Boundary Layer Meteorology.* Kluwer Academic Publishers, 666 pp.

Wyngaard, J. C., 1992: Atmospheric turbulence. *Annu. Rev. Fluid Mech.,* **24,** 205–233.

——, and R. A. Brost, 1984: Top-down and bottom-up diffusion of a scalar in the convective boundary layer. *J. Atmos. Sci.,* **41,** 102–112.